

See discussions, stats, and author profiles for this publication at: <https://www.researchgate.net/publication/268221999>

Fano Resonances in Compositional Clusters of Aluminum Nanodisks at the UV Spectrum: a Route to Design Efficient and Precise Biochemical Sensors

ARTICLE *in* PLASMONICS · DECEMBER 2014

Impact Factor: 2.24 · DOI: 10.1007/s11468-014-9762-8

CITATIONS

9

READS

47

2 AUTHORS:



Saeed Golmohammadi

University of Tabriz

58 PUBLICATIONS 178 CITATIONS

[SEE PROFILE](#)



Arash Ahmadvand

Florida International University

48 PUBLICATIONS 111 CITATIONS

[SEE PROFILE](#)

Fano Resonances in Compositional Clusters of Aluminum Nanodisks at the UV Spectrum: a Route to Design Efficient and Precise Biochemical Sensors

Saeed Golmohammadi · Arash Ahmadvand

Received: 30 April 2014 / Accepted: 16 July 2014 / Published online: 9 August 2014
© Springer Science+Business Media New York 2014

Abstract In this study, we have investigated the plasmon resonance coupling between proximal compositional Al nanoparticles that are organized in a closely spaced molecular orientation as nanoclusters. Plasmon hybridization model is employed as a theoretical model to study the spectral response of the proposed nanostructures. The optical properties of trimer, heptamer, and octamer clusters based on Al/Al₂O₃ nanodisks are evaluated using finite-difference time-domain (FDTD) model numerically. We have proved that a constructive and weak interference between subradiant dark and superradiant bright modes as the plasmon resonance modes causes the appearance of strong Fano resonances at the spectral response of the heptamer and octamer clusters at the UV spectrum. The effects and results of the structural and chemical modifications in the proposed nanoclusters have been discussed and determined. Finally, illuminating an octamer cluster composed of Al/Al₂O₃ nanoparticles and simultaneous modifications in the refractive index of the dielectric environment lead to dramatic changes in the position and quality of the Fano dip. Plotting a linear figure of merit (FoM) for the proposed octamer and quantifying this parameter for the structure as 7.72, we have verified that the structure has a strong potential to be used in designing precise localized surface plasmon resonance (LSPR) sensors that are able to sense minor environmental perturbations with high accuracy. Proposed clusters composed of Al/Al₂O₃ provide an opportunity to design and fabricate low-cost, high responsivity,

tunable, and CMOS-compatible devices and efficient biochemical sensors.

Keywords Aluminum nanoparticles · UV spectrum · Fano resonance · Plasmon resonance · Figure of merit (FoM)

Introduction

Surface plasmons in noble metallic nanoparticles (NPs) have extensively been considered and employed in designing numerous optic-based structures and devices in nanoscale dimensions [1–5]. The substance and the shape of utilized NPs play key roles in designing and fabricating efficient, tunable, high responsivity, and advanced structures such as nanoantennas, switches, photovoltaics, biosensors, and surface-enhanced Raman spectroscopy (SERS) devices [6–12]. Considering the characteristics of metallic NPs from the chemical point of view, gold (Au), silver (Ag), and copper (Cu) are the fundamental metallic components that have a wide range of usage in plasmonic concepts [13, 14]. It has been strongly verified that plasmon resonances in subwavelength dimensions can be easily tuned from visible to near infrared region (NIR) and even longer wavelengths [13, 15]. On the other hand, due to the intrinsic limitations in the chemical characteristics of well-known noble metals, therefore, providing plasmon resonances at UV wavelengths is highly difficult and challenging. It is confirmed that Ag is the sole famous noble metal that is able to support severe plasmon resonances from $\lambda \sim 340$ nm to the visible spectrum, but rapid oxidation is the main disadvantage of Ag which causes dramatic decrements in plasmonic features. Besides, due to the strong dissipative behavior of Au nanoparticles, which originates from the interband transitions inside the metallic component, this material is not able to support strong plasmon resonances shorter than visible wavelengths (actually

S. Golmohammadi
School of Engineering-Emerging Technologies, University of Tabriz,
Tabriz 516614761, Iran

A. Ahmadvand (✉)
Young Researchers and Elite Club, Ahar Branch, Islamic Azad
University, Ahar, Iran
e-mail: a_ahmadvand@iau-ahar.ac.ir

$\lambda < 540$ nm) [16, 17]. Newly, Knight et al. [18] have verified that aluminum (Al) can be considered as an alternative plasmonic material across the UV to visible spectrum. This work also has demonstrated that the dipole and quadrupole extremes can be observed along the scattering profile at the mentioned bandwidths using far-field spectroscopy approach. As a result, in employing Al oxide (Al_2O_3) as a cover layer and using a SiO_2 substance as substrate layer for a certain nanostructure, plasmon resonance peaks can be adjusted at desired wavelengths with acceptable amplitudes.

Plasmon hybridization theory has been advised to characterize the spectral response and plasmonic features of two- and three-dimensional NP clusters in diverse molecular orientations. On the other hand, hybridization of plasmon resonance modes in a closely spaced Al NPs has not been studied entirely yet. Today, simple and complex nanoclusters in various molecular designations have extensively been introduced and studied numerically and experimentally [19, 20]. It is well understood that these clusters are able to support strong electric and magnetic plasmon and Fano resonances (FRs) in their subwavelength geometries at visible to mid-infrared spectrum. Metallic NPs in heptamer, octamer, tetramer, decamer, hexamer, and necklace formations are some of the important and well-known NP aggregates that have a wide range of utilization in designing nanophotonic and integrated optical devices [21–24]. From the technical point of view, illuminating one of the mentioned symmetric plasmonic clusters (e.g., heptamer) by a linear light source, then calculating relevant plasmon response and drawing the extinction profile, pronounced superradiant bright mode and a subradiant dark mode regarding dipolar and multipolar plasmon resonance modes are appeared. Overlap of these modes and constructive interference between them lead to the appearing of FR dip in intense and weak regimes along the scattering cross-sectional profile [25, 26]. Studies have demonstrated that FR position and performance can be transmuted positively by the possible symmetry breaking in the cluster structure dramatically [26, 27]. It should be noted that asymmetry causes appearing of some destructive and constructive results, for instance, from the positive point of view, extremely fast, efficient, and high responsivity plasmonic Fano switches and plasmonic sensors can be designed and fabricated based on this symmetry breaking [28]. Despite these advantages, difficulty in fabrication and highly complex theoretical analysis are the negative aspects of this symmetry breaking. Prior works also have verified that single and multiple Fano dips can be formed by several kinds of NP clusters at the visible and NIR spectrum. In order for FRs to appear at the UV spectrum, this unique opportunity can be employed in numerous applications and purposes such as sensing, switching, photodetection, and SERS applications.

In this study, we show that Al NPs with a certain covering of Al oxide layer in a few nanometers can be used in designing NP clusters. Moreover, we measure the optical response and plasmonic properties of a simple trimer composed of Al/ Al_2O_3

NPs deposited on a silica substrate. Then, the same procedure for a more complex cluster (heptamer) is applied and repeated to seek for high quality FR dips. Finally, we determine the Al nanodisk purity to obtain narrow Fano dip at UV to visible spectrum by the optimal NP cluster. These characteristics of Al NPs open new paths to provide efficient, low-cost, tunable, and CMOS-compatible devices such as localized surface plasmon resonance (LSPR) sensors that are able to sense extremely minor variations in the short wavelengths with acceptable accuracy.

Results and Discussion

To calculate the spectral response of Al-based nanoclusters, we first discuss FR generation when interacting opposite dark and bright modes briefly. From the Fano resonance viewpoint, two major modes participate in formation of a Fano dip: the superradiant bright mode which corresponds to the in-phase oscillation of dipolar plasmon resonance of all nanoparticles and the subradiant dark mode related to the plasmon dipolar moment of the central particle which is in oppose oscillation direction of proximal particles dipolar moments. It is well accepted that in the nonretarded limit, the subradiant mode cannot be coupled to the superradiant mode efficiently, and on the other side, in the retarded limit, a constructive and weak interaction between dark and bright modes can occur, which contains a Fano resonance in the superradiant continuum at the energy level of the superradiant mode. Figure 1a shows a schematic diagram of the operating wavelength and plasmon tuning range for four different metals (Au, Ag, Cu, and Al) that can be considered as candidate substances for plasmonic applications. Comparing indicated

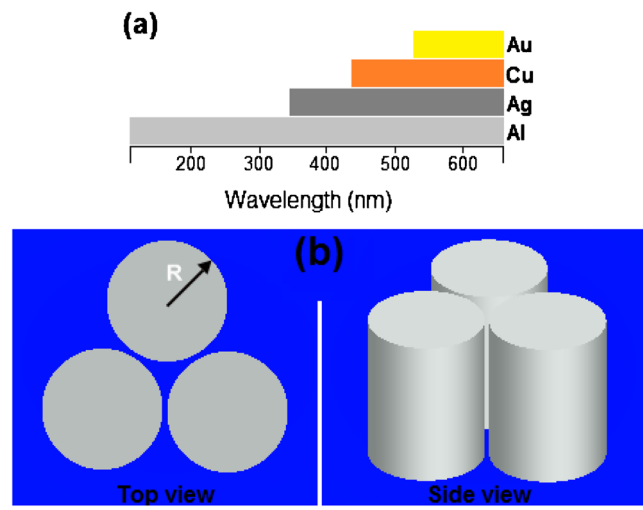


Fig. 1 **a** Plasmon tuning domain of three regular plasmonic substances (Au, Ag, and Cu) that are compared with aluminum; **b** schematic diagrams of *top* and *side* views of Al NPs as a trimer cluster. The radii of NPs are identical and located at a certain gap distance from each other (D_{3h})

metals, obviously, Al is able to function at the UV spectrum effectively. Figure 1b illustrates the top and side views of a simple and systematic trimer composed of three pure Al nanodisks that are situated in a close proximity to each other with an identical gap distance of 4 nm. Considering the determined geometrical results by Knight et al. [18] for an isolated Al nanodisk, we have calculated and have drawn the spectral response for a trimer cluster in Fig. 2 using finite-difference time-domain (FDTD) method as a numerical tool. Accordingly, the height of the cluster is considered as an infinite parameter, and the substrate of the cluster is SiO_2 layer with the permittivity of $\epsilon=2.1$. The employed material

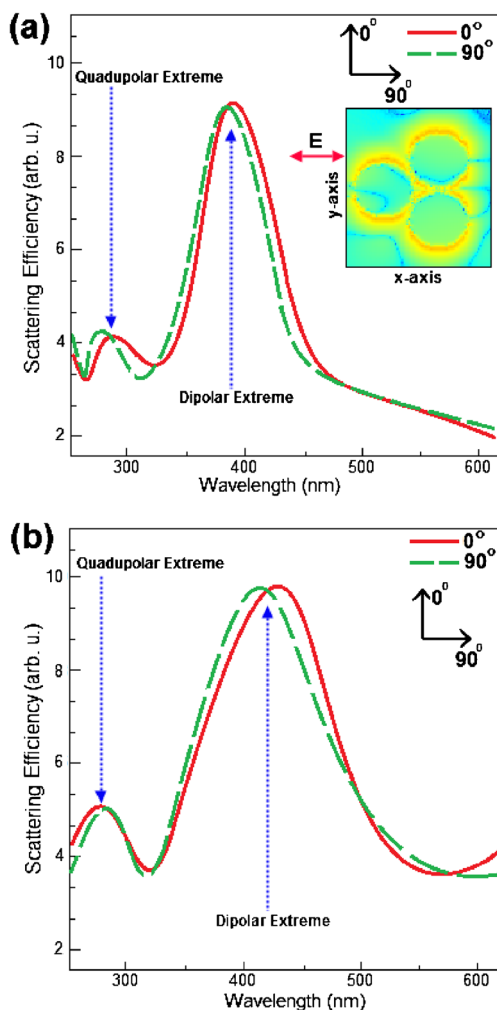


Fig. 2 **a** Calculated scattering spectra for a trimer based on pure Al nanodisks with a radii of $R=45$ nm; the gap distance is 4 nm, and the height of the particles are infinite during illuminating by transverse and longitudinal polarizations. As a result, two peaks regarding to the dipole and quadrupole plasmon resonance modes have been appeared at the short and longer spectra. *Inset* snapshot shows the plasmon excitation in proposed trimer under illuminating by an incident transverse polarization. **b** Scattering efficiency profile is calculated for the pure Al NPs with the radii of $R=65$ nm and the same gap distance. A subtle red-shift in the position of superradiant bright mode has been taken place, while the situation of subradiant mode remains unchanged

of NPs is pure Palik Al and the radii of NPs are variant, and we changed it in the range of 45 to 65 nm. For each one of the individual clusters, the polarization direction of the incident electromagnetic waves (EM) is variant, and the results for two different angles (0° and 90°) have been sketched in relevant profiles. Figure 2a, b illustrates the scattering efficiency profile for the proposed Al trimer for two different NP sizes and different polarizations. Noticing in Fig. 2a that is calculated for a trimer composed of Al NPs with a radius of 45 nm, we detected an extreme at $\lambda\sim385$ nm which corresponds to the dipolar plasmon resonance mode and a small peak at $\lambda\sim270$ nm relating to the quadrupolar resonance mode. The quadrupole resonance is a subradiant dark mode which cannot be strongly coupled to the external field; therefore, the amplitude and efficiency of this mode are low and will not be able to supply FR dip at the scattering profile. Inset figure demonstrates a two-dimensional snapshot of plasmon resonance excitation under incident longitudinal electric polarization mode illumination. Increasing the size of Al NPs in the trimer cluster to $R=65$ nm (Fig. 2b), a subtle red-shift in dipolar peak is observed ($\lambda\sim430$ nm), while the quadrupolar extreme is almost fixed ($\lambda\sim275$ nm). Also, the amplitude of both of the resonance modes has been increased dramatically in comparison with the smaller trimer. More increments in the size of the NPs cause the red-shift of plasmon resonances to the longer spectrum (visible), while the amplitude is reducing due to the absorption of EM fields. Therefore, in this regime, the possibility of strong coupling between dark and bright modes is reduced noticeably. To calculate and determine the dielectric response of the employed Al NPs to various depositions and material add-ons (e.g., Al_2O_3), three-dimensional FDTD method is utilized, and consequently, we employed an incident spectrum with the polarization angles of 0° to 90° and the bandwidths of $\lambda=150\text{--}800$ nm to study this condition. Table 1 includes all of the applied settings and parameters which describe the numerical FDTD model. Here, the dielectric function of Al NPs for each one of the employed materials is derived from the ellipsometric

Table 1 FDTD model settings and parameter descriptions

Parameter	Description
Spatial cell sizes ($dx=dy=dz$)	0.01 nm
Number of cells	12,000
Number of time steps (dt)	8,000
Simulation time	3,900 fs
Number of snapshots	12,792
Background index	1
Boundary conditions	Perfectly matched layers (PML)
Number of PML layers	16

data, considering a bilayer multiplex of a narrow dielectric oxide layer covering an infinite thick Al layer, which is specified by the modified Drude model [29–31]:

$$\varepsilon_{\text{Al}} = \varepsilon_{\infty} - \frac{\omega_p^2}{\omega^2 + i\gamma\omega} \quad (1)$$

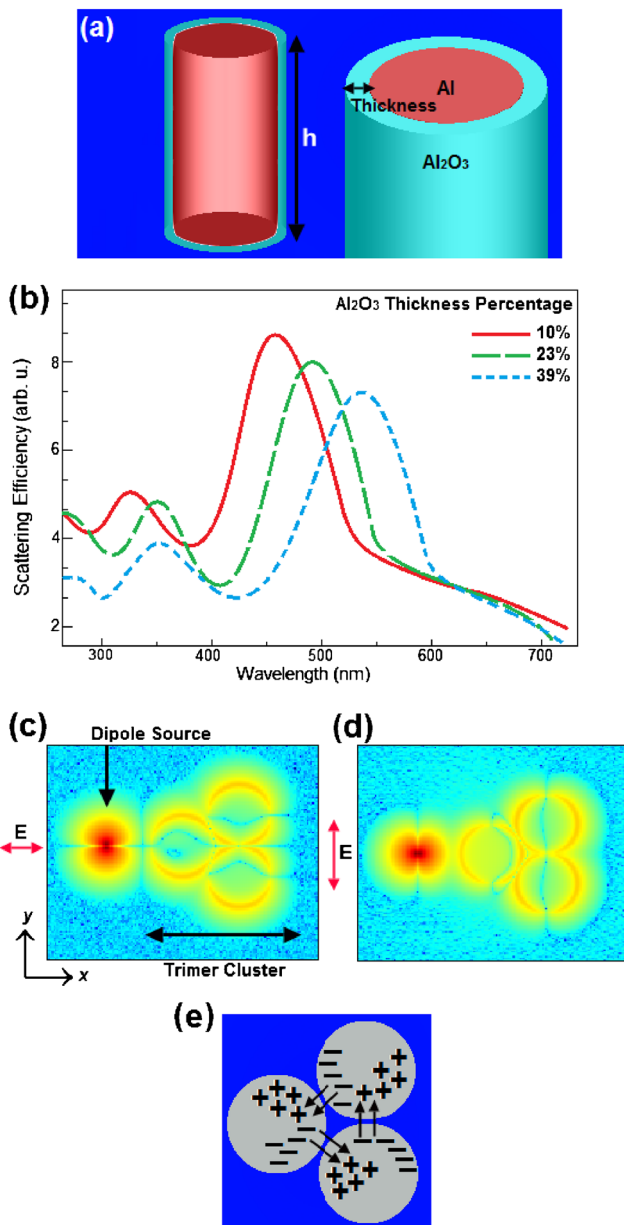


Fig. 3 **a** Schematic diagram of an Al nanodisk covered by an oxide layer (Al_2O_3) with variable thickness size. **b** Scattering efficiency diagram for a trimer composed of Al NPs that are covered by an oxide layer. Increasing the oxide layer thickness (percentage), the dipolar, and quadrupolar extremes red-shifts to longer spectra, while the amplitude of peaks decreases. **c**, **d** Two-dimensional snapshots of the plasmon resonance excitation in a compositional trimer under transverse and longitudinal polarizations. **e** Charge density distribution between trimer NPs during excitation by an incident light

where ω_p is the bulk plasmon frequency, γ is the damping constant, and ε_{∞} is the high-frequency response. In simulation model, the thickness of the Al_2O_3 layers is identical to each other and has been set to the range of 5–10 nm, ε_{∞} is approximately ~6–7, and the metallic Drude damping constant is in the range of γ ~0.7–14.9 eV. It has already been verified that utilizing Bruggeman's model [18] allows calculating the dielectric function for a compositional arrangement such as our proposed nanostructure in the current study ($\text{Al}/\text{Al}_2\text{O}_3/\text{SiO}_2$). Moreover, the effects of the oxide (Al_2O_3) layer which has grown around the NPs and the presence of the dielectric substrate (SiO_2) on spectral response of the compositional nanostructure are described numerically. To this end, we study the effect of Al_2O_3 layer on quadrupole and dipole plasmon resonance modes in the scattering efficiency profile. Figure 3a illustrates a schematic diagram for an isolated Al disk that is encompassed by an oxide layer with the height of h (infinite parameter). Figure 3b shows the results of modifications in the oxide thickness in the range of 10 to 39 % on plasmonic response of a trimer with radii of $R=65$ nm and an identical gap distance ($D_{3h}=4$ nm). Noticing in the scattering efficiency diagram, dipolar and quadrupolar peaks appear for superradiant and subradiant plasmon resonance modes, respectively.

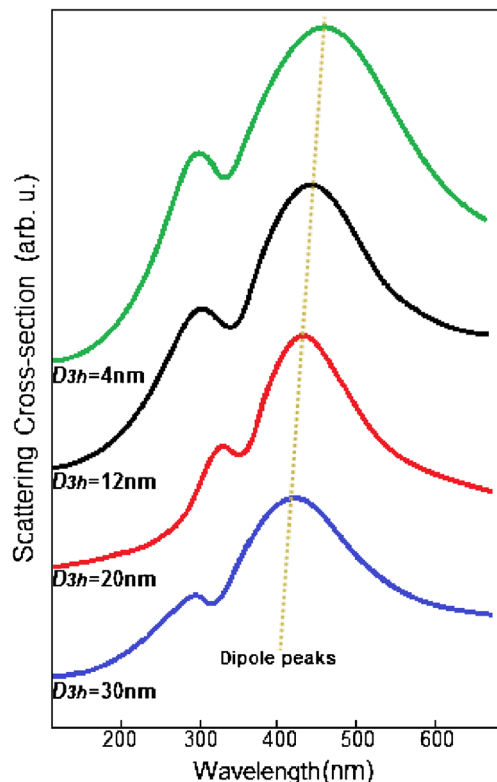
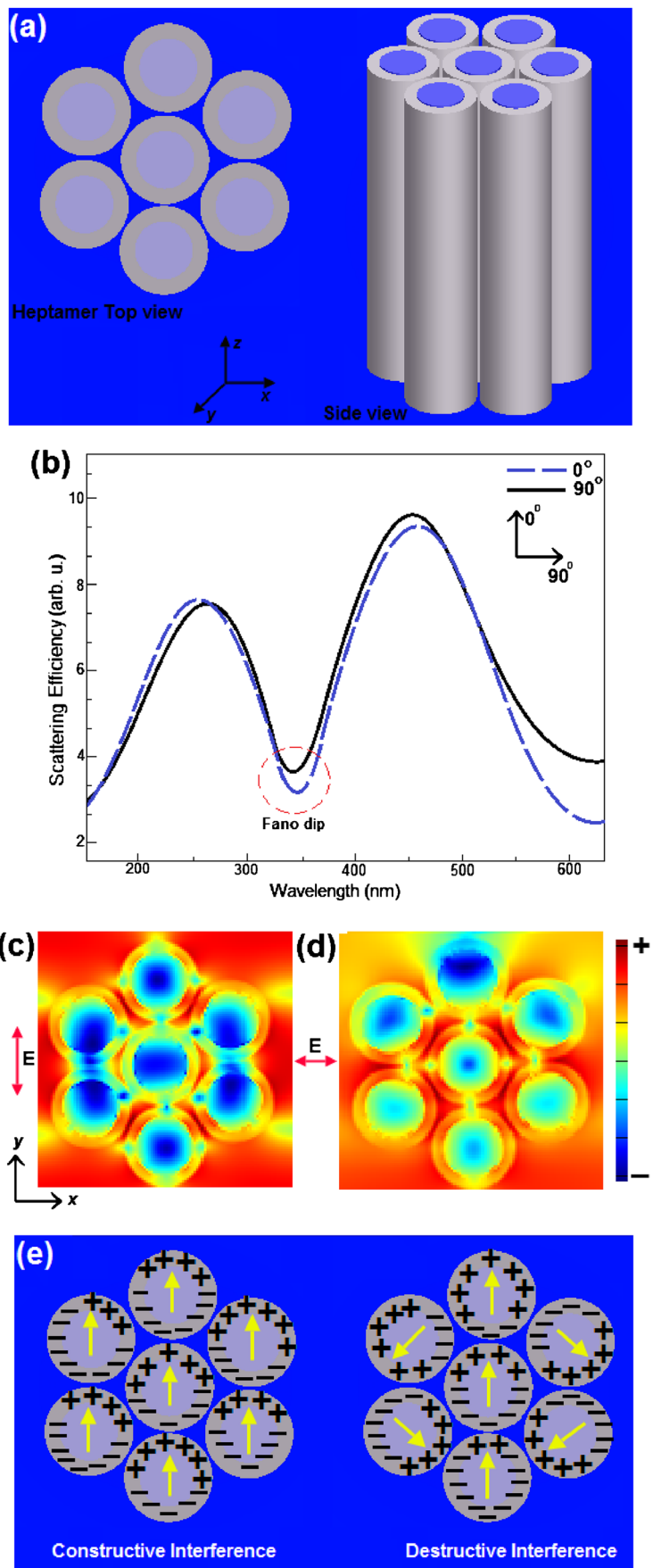


Fig. 4 Calculated scattering cross-sectional diagram for an Al NP-based trimer with the radii of $R=65$ nm, while the gap distance between proximal particles is variant. Decreasing the gap distance red-shifts the dipole resonance mode to longer spectra and the quadrupole extreme becomes stronger and appears with this gap distance decrement. The amplitude of dipolar mode is increased as well

Fig. 5 **a** Schematic diagram of a compositional Al/Al₂O₃ nanodisks heptamer in *side* and *top* views; calculated scattering spectra for the proposed Al-based heptamer under transverse and longitudinal polarizations. Deep Fano minima are observed at the $\lambda \sim 340$ nm. **c, d** Two-dimensional (xy) snapshots for the transverse and longitudinal polarization modes. Strong plasmon resonance coupling between proximal NPs is obvious. **e** Charge density distribution plotted for constructive and destructive interferences between Al NPs in a cluster



Increasing the ratio of covering oxide layer, plasmon resonance peaks are red-shifted to the longer wavelengths, and the amplitude of the scattering extremes became wider. For instance, for the examined trimer composed of NPs with an oxide thickness of approximately 39 %, the dipole and the quadrupole peaks are observed at $\lambda=449$ nm and $\lambda=251$ nm. Figure 3c, d demonstrates two-dimensional snapshots of plasmon resonance excitation under transverse and longitudinal polarization modes for the examined trimer composed of Al NPs with radii of $R=65$ nm and 30 % oxide layer. Figure 3e exhibits the density distribution variation between NPs inside the trimer during resonance coupling. As a final examination, regarding the spectral response of an Al-based trimer, the effect of alterations in the gap distance between proximal NPs is drawn in Fig. 4. Accordingly, in altering the gap distance in the range of 30 to 4 nm for a big gap distance, the quadrupolar peak of subradiant dark mode becomes weak, and a distinct peak related to the superradiant bright mode appears along the scattering cross-sectional profile. As a result, in reducing the gap distance, dipolar extreme is red-

shifted to the longer wavelengths and multipolar extremes become stronger. It is well known that strong dark and bright modes and constructive interference between these modes directly leads to the emerging of a robust Fano dip. To this end, we change the orientation of the examined trimer to a symmetric and more complex molecular plasmonic cluster: the heptamer. Due to the number of NPs and inherent symmetricity of a heptamer cluster, the possibility of FR observation in Al/Al₂O₃/SiO₂-based cluster is noticeable and high. Considering the obtained geometrical sizes, compositional settings, and quantities for Al NPs, Fig. 5a demonstrates a schematic diagram of the proposed heptamer for both sides and top views. Numerically, computed and driven spectral response for the nanostructure is illustrated in Fig. 5b under illuminating by an incident electric dipole source in transverse (0°) and longitudinal (90°) polarization modes. Strong coupling between superradiant and subradiant resonance modes causes the appearing of deep Fano minima at short wavelengths ($\lambda\sim 340$ nm), and two extremes regarding the quadrupolar and dipolar plasmon resonances are appeared at $\lambda\sim 260$

Fig. 6 **a** Calculated scattering cross-sectional diagram for an Al/Al₂O₃ NP-based heptamer with the variant radii size. Increasing the size of nanodisks leads to red-shift of Fano minima, and as result, FR minima become broaden. **b** Scattering cross-sectional diagram for a heptamer with the variable gap distance size is depicted numerically. Increasing the size gap distance causes to blue-shift of FR, and consequently, the Fano minima becomes intensely broadened and disappear

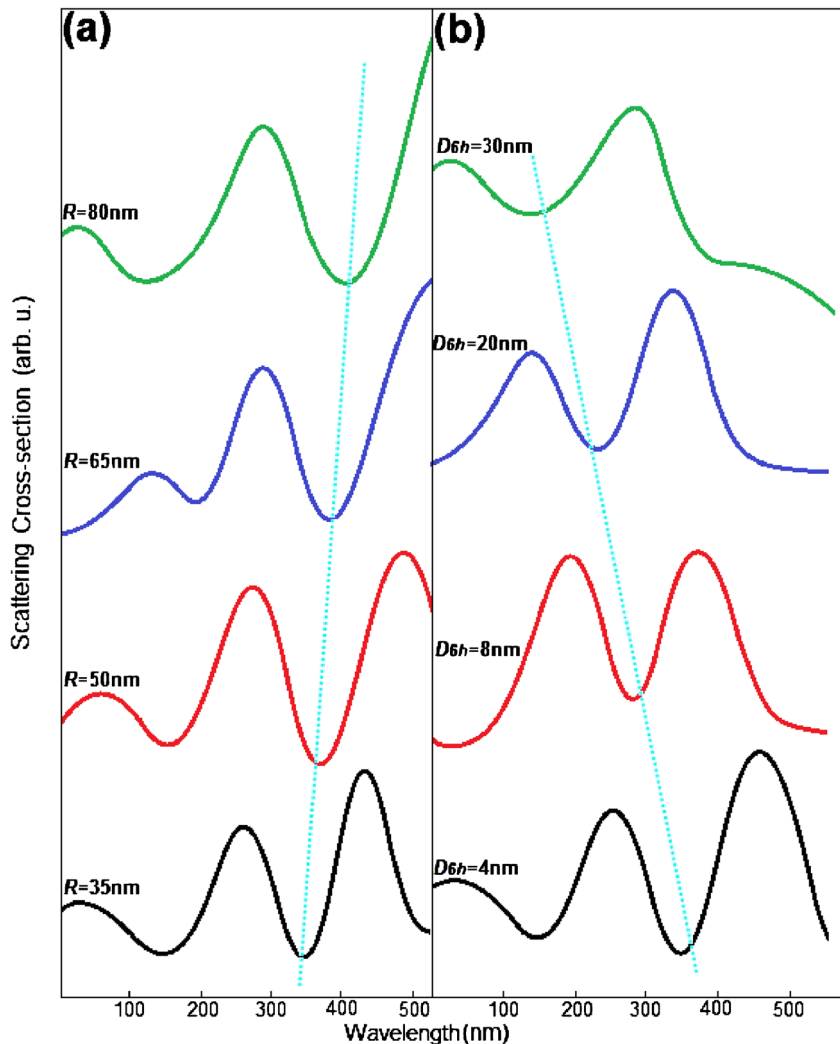
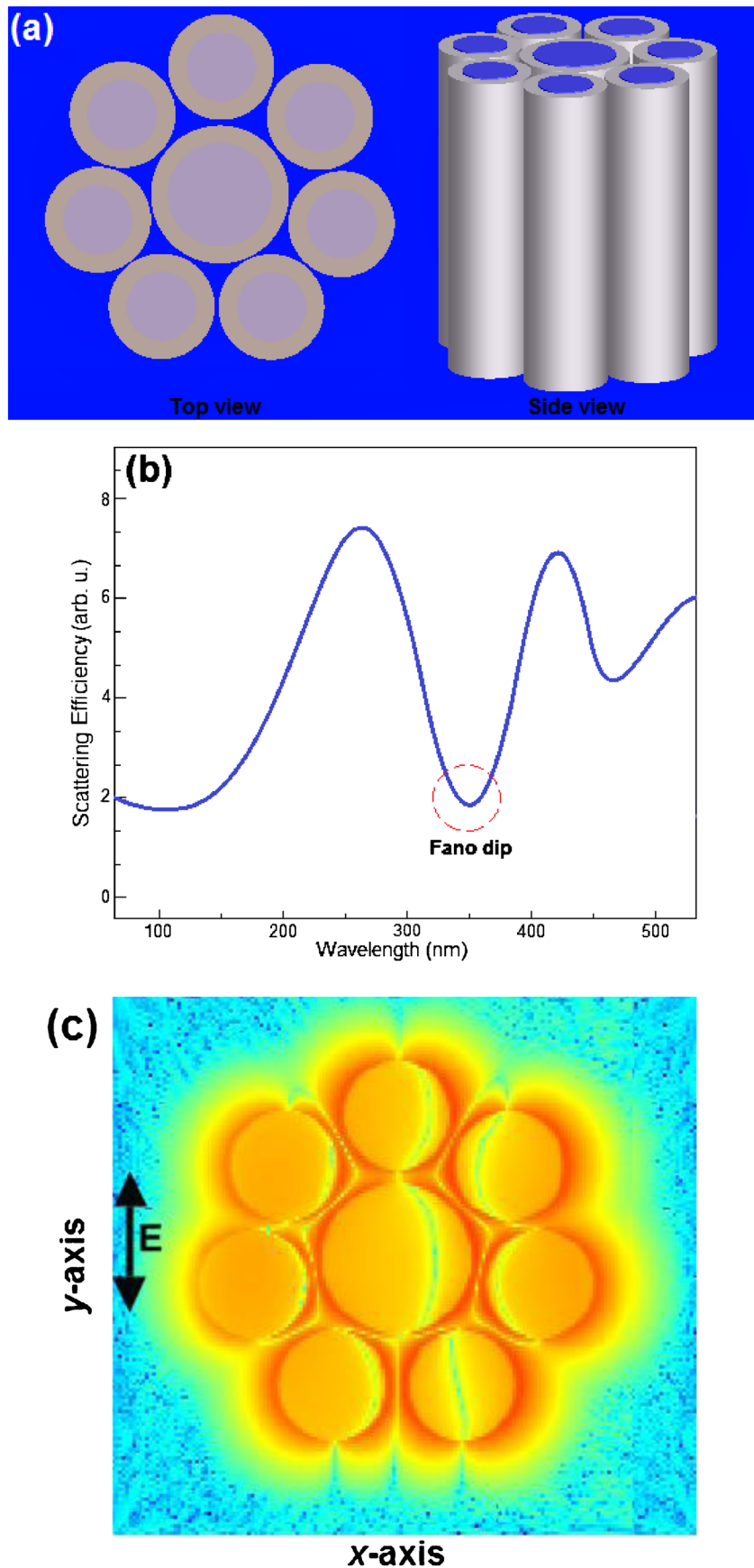


Fig. 7 **a** Schematic diagram of the proposed Al/Al₂O₃ NP-based octamer in *top* and *side* views that is deposited on a SiO₂ host material. The size of peripheral NPs are identical, while the size of central particle is bigger in comparison to them. **b** Calculated scattering spectra for an Al/Al₂O₃/SiO₂ NP-based octamer, and a Fano minimum has been appeared at the $\lambda=352$ nm. **c** Two-dimensional snapshot of the proposed octamer under illuminating by an incident transverse electric polarization mode



and 470 nm, respectively. Technically, Fano dip here can be characterized by suppression of the superradiant mode (at the $\lambda \sim 470$ nm). Charge density distribution through the heptamer cluster composed of Al NPs is depicted for constructive and destructive interferences between bright and dark modes (see Fig. 5e). The noteworthy point in this figure is the same direction for the constructive interference of radiated fields. In contrast, in the destructive interference regime, the charge oscillation directions are completely opposite.

Next, we examine the quality of FR minima (depth and narrowness) for the structural modifications in the compositional Al-based heptamer. First, we increase the radii of employed NPs, while the percentage of the oxide layer is constant as 30 % and the gap distance is 4 nm. Figure 6a demonstrates the calculation results in a scattering cross-sectional diagram. Obviously, by increasing the size of NPs, the Fano dip position is red-shifted to the longer spectra and becomes broader and deeper. Therefore, utilizing Al/Al₂O₃ nanodisks with identical radii in the range of $R=35\text{--}60$ nm is an optimal choice to support severe FRs at the UV spectrum. On the other hand, increasing the gap distance between neighbor NPs of the heptamer directly blue-shifts the Fano minima to the shorter spectra (see Fig. 6b). In this investigation, the final radii of NPs are determined as $R=60$ nm and the percentage of oxide layer is 30 %.

In continuation, we study the localized surface plasmon resonance (LSPR) sensing performance by a complex cluster composed of Al/Al₂O₃ nanodisks during the making modifications in the dielectric medium. To this end, we employ an octamer cluster composed of eight NPs based on the achieved parametrical sizes in the earlier studies. Figure 7a illustrates a schematic diagram of an octamer based on compositional nanodisks. It should be noted that the size of peripheral NPs are identical and have been settled to $R=60$ nm with a gap distance of 4 nm, while the central particle is bigger which provides a required asymmetry to appearing of Fano dip along the scattering profile. Therefore, the size of central NP has been settled to $R=75$ nm with the same gap size to proximal peripheral NPs. Also, the ratio of the oxide layer is 30 % for all of the NPs proportional to their radii individually. Then, in illuminating the examined octamer by an incident transverse electric dipole source (Fig. 7b), a deep and almost narrow Fano minima appear at UV spectra ($\lambda=352$ nm). Figure 7c is a two-dimensional snapshot of the plasmon resonance excitation in proposed Al/Al₂O₃ NP-based octamer under transverse electric (dipole source) polarization mode. It has extensively been investigated that the behavior of FR (position, depth, and narrowness) can be exploited in designing ultra-sensitive multiwavelength LSPR sensors. Several structures composed of metallic NPs have been employed in designing LSPR sensors which are working based on FR performance. On the other hand, high sensitivity to the environmental dielectric modifications is one of the major goals that has been considered in

designing LSPR sensing configurations. Most of these works have considered the Fano position at the visible to the near infrared spectrum. The ability to sensing the plasmon resonance at the UV spectrum is remarkable. To measure and determine the LSPR sensitivity of the proposed octamer composed of Al//Al₂O₃ NPs, corresponding linear figure of merit (FoM) must be sketched and quantified. Plasmon resonance energy differences (ΔE eV) between the maximum and minimum energy levels over the refractive index variations is the key factor in computation and drawing of FoM. Hence, we change the dielectric environment based on various refractive indices by changing the surrounding substances. Consequently, we plotted the scattering cross-sectional diagram for the examined octamer numerically in Fig. 8a. In this figure also, we compared the plasmonic response of the structure to the variations in the surrounding medium as follows: CH₃OH (ethanol) $n=1.331$, C₄H₁₀O (butanol) $n=1.399$, and BK7 matching liquid (similar to Cargille immersion oil type B that is measured in Cargille laboratory) ($n=1.516$). In all of the simulation steps, we assumed that the examined octamer is immersed by the mentioned dielectric liquid materials thoroughly. Figure 8a demonstrates the results of this environmental modification process. Notice that in this figure, increasing the refractive index of the dielectric material red-shifts the Fano dip to the longer spectra, while the FR position remains at the UV region.

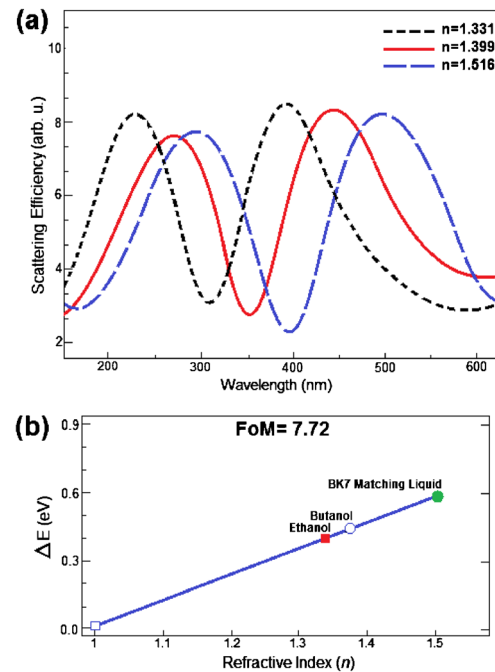


Fig. 8 a Calculated scattering cross-sectional diagram for an Al/Al₂O₃/SiO₂ NP-based octamer cluster during environmental modifications. Increasing the refractive index of environmental dielectric substance red-shifts the Fano minima and FR minima becomes narrower and deeper. b Calculated linear figure of merit (FoM) which is plotted for the dimer shape structure to quantify the LSPR sensitivity

In this regime, a pronounced Fano dip is generated at $\lambda=394$ nm for the medium with the refractive index of $n=1.516$. To determine the sensitivity of LSPR for the elucidated octamer structure, we divided the slope of linear regression by resonance line width 0.103 eV, and as a result, the FoM is determined as 7.72 (Fig. 8b). Comparing analogous NP clusters with different substances (e.g., gold and silver) with the proposed aluminum clusters, the LSPR sensitivity of the examined configuration is remarkable. The proposed cluster can be fabricated lithographically with smaller gaps between the Al-NPs which supplies acceptable accuracy during sensing purposes. The studied cluster has a strong potential to be utilized in designing precise biochemical sensors that are able to recognize ultra-short wavelengths with remarkable FoM. Moreover, this structure yields low-cost, efficient, and CMOS-compatible sensors and analogous nanostructures. All of the chemical and physical properties regarding the Al_2O_3 (oxide layer) have been considered based on proposed data in [32–34].

Conclusions

In this work, we investigated the hybridization of plasmon resonance modes between closely spaced Al NPs that are suited in a close proximity to each other as a nanocluster. Utilizing an oxide layer (Al_2O_3) as a coverage for the Al nanodisk, we examined and calculated the optical response and scattering cross-sectional profile for a simple trimer composed of three Al/ Al_2O_3 nanodisks. Also, in this method, we determined the effect of oxide layer thickness proportional to the size of the NP on the Fano minima performance. As a result, dipolar and quadrupolar plasmon resonance modes have been appearing at the UV spectra with dramatic amplitudes in efficiency diagram. Extending the number of particles, we designed a symmetric heptamer based on Al/ Al_2O_3 NPs that are deposited on a SiO_2 substrate. The possibility of FR observation has been evaluated by illuminating the structure under longitudinal and transverse polarization modes excitations. In changing the Al-based conventional heptamer array to a more complex molecular structure (octamer), we studied the plasmon resonance and FR behavior for the new structure numerically. By employing final Al-based structure for sensing application, the LSPR sensitivity for the structure has been evaluated. We proved that by applying minor modifications in the refractive index of the environmental dielectric substance, the position, depth, and narrowness of FR can be affected significantly. Through plotting and quantifying corresponding FoM (7.72) for the final octamer, we examined the plasmon resonance sensitivity of the structure.

References

- Raether H (1988) Surface plasmons on smooth and rough surfaces and on gratings. Springer, Berlin
- Kreibig U, Vollmer M (1995) Optical properties of metal clusters. Springer, Berlin
- Maier SA (2007) Plasmonics: fundamentals and applications. Springer, New York
- Saleh BEA, Teich MC (1991) Fundamentals of photonics. Wiley, New York
- Barnes WL, Dereux A, Ebbesen TW (2003) Surface plasmon sub-wavelength optics. *Nature* 424:824–830
- Linic S, Christopher P, Ingram DB (2011) Plasmonic-metal nanostructures for efficient conversion of solar to chemical energy. *Nat Mater* 10:911–921
- Atwater HA, Polman A (2010) Plasmonics for improved photovoltaic devices. *Nat Mater* 9:205–213
- Campion A, Kambhampati P (1998) Surface-enhanced Raman scattering. *Chem Soc Rev* 27:241–250
- Rakic AD, Djurisic AB, Elazar JM, Majewski ML (1998) Optical properties of metallic films for vertical-cavity optoelectronic devices. *Appl Opt* 37:5271–5283
- Knight MW, Sobhani H, Nordlander P, Halas NJ (2011) Photodetection with active optical antennas. *Science* 332:702–704
- Hsiao VKS, Zheng YB, Krishna B, Huang TJ (2008) Light-driven plasmonic switches based on Au nanodisk arrays and photoresponsive liquid crystals. *Adv Mater* 20:3528–3532
- Ming T, Zhao L, Xiao M, Wang J (2010) Resonance-coupling-based plasmonic switches. *Small* 6:2514–2519
- Maier SA, Brongersma ML, Kik PG, Meltzer S, Requicha AAG, Atwater HA (2001) Plasmonics: a route to nanoscale optical devices. *Adv Mater* 13:1501–1505
- Pelton M, Aizpurua J, Bryant G (2008) Metal-nanoparticle plasmonics. *Laser Photonics Rev* 2:136–159
- Xi ZH, Ying G, Huang GQ (2008) A visible-near infrared tunable waveguide based on plasmonic gold nanoshell. *Chin Phys B* 17:2567–07
- Ono A, Kikawada M, Akimoto R, Inami W, Kawata Y (2013) Fluorescence enhancement with deep-ultraviolet surface plasmon excitation. *Opt Express* 21:17447–17453
- McMahon JM, Schatz GC, Gray SK (2013) Plasmonics in the ultraviolet with the poor metals Al, Ga, In, Sn, Tl, Pb, and Bi. *Phys Chem Chem Phys* 15:5415–5423
- Knight MW, King NS, Liu L, Everitt HO, Nordlander P, Halas NJ (2014) Aluminum for plasmonics. *ACS Nano* 8:834–840
- Prodan E, Radloff C, Halas NJ, Nordlander P (2003) A hybridization model for the plasmon response of complex nanostructures. *Science* 302:419–421
- Fan JA, Wu C, Bao K, Bao J, Bardhan R, Halas NJ, Manoharan VN, Nordlander P, Shvets G, Capasso F (2010) Self-assembled plasmonic nanoparticle clusters. *Science* 328:1135–1138
- Yan B, Boriskina SV, Reinhard BM (2011) Optimizing gold nanoparticles cluster configurations ($n \leq 7$) for array applications. *J Phys Chem C* 115:4578–4583
- Liu S-D, Yang Z, Liu R-P, Li X-Y (2012) Multiple Fano resonances in plasmonic heptamer clusters composed of split nanorings. *ACS Nano* 6:6260–6271
- Sönnerup C, Reinhard BM, Liphardt J, Alivisatos AP (2005) A molecular ruler based on plasmon coupling of single gold and silver nanoparticles. *Nat Biotechnol* 23:741–745
- Pasquale AJ, Reinhard BM, Dal Negro L (2011) Engineering photonic-plasmonic coupling in metal nanoparticle necklaces. *ACS Nano* 5:6578–6585
- Luk'yanchuk B, Zheludev NI, Maier SA, Halas NJ, Nordlander P, Giessen H, Chong CT (2010) The Fano resonance in plasmonic nanostructures and metamaterials. *Nat Mater* 9:707–715

26. Hao F, Sonneneck Y, Dorpe PV, Maier SA, Halas NJ, Nordlander P (2008) Symmetry breaking in plasmonic nanocavities: subradiant LSPR sensing and tunable Fano resonances. *Nano Lett* 8:3983–3988
27. Miroshnichenko AE, Flash S, Kivshar YS (2010) Fano resonances in nanoscale structures. *Rev Mod Phys* 82:2257
28. Chang W-S, Lassiter JB, Swanglap P, Sobhani H, Khatua S, Nordlander P, Halas NJ, Link S (2012) A plasmonic Fano switch. *Nano Lett* 12:4977–4982
29. Palik ED (1998) Handbook of optical constants. Academic, San Diego
30. Choy TC (1999) Effective medium theory: principles and applications. Oxford University, Oxford
31. Tsang L, Kong JA, Ding K-H (2000) Scattering of electromagnetic waves: theories and applications. Wiley, USA
32. Archer DG (1993) Thermodynamic properties of synthetic sapphire (α -Al₂O₃), standard reference material 720 and the effect of temperature-scale differences on thermodynamic properties. *J Phys Chem Ref Data* 22:1441
33. Kim Y, Lee SM, Park CS, Lee SI (1997) Substrate dependence on the optical properties of Al₂O₃ films grown by atomic layer deposition. *Appl Phys Lett* 71:3604–3606
34. Park BG, Crosky AG, Hellier AK (2001) Material characterization, and mechanical properties of Al₂O₃-Al metal matrix composites. *J Mater Sci* 36:2417–2426